Quantum-mechanical description of ionization, capture, and excitation in proton collisions with atomic oxygen

T. Kirchner,[1,2] H. J. Lüdde,[2] M. Horbatsch,[1] and R. M. Dreizler[2]
[1]*Department of Physics and Astronomy, York University, Toronto, Ontario, Canada M3J 1P3*
[2]*Institut für Theoretische Physik, Universität Frankfurt, Robert-Mayer-Straße 8, D-60054 Frankfurt/Main, Germany*
(Received 7 December 1999; published 11 April 2000)

The basis generator method is used to propagate effective single-particle equations for ion-atom collisions to provide a mean-field description for the proton-oxygen collision system. The pure capture and ionization as well as transfer ionization cross sections are calculated using two alternative prescriptions to extract the physical information from the propagated orbitals. The sensitivity of the resonant single capture cross section to the effective single-particle potential for atomic oxygen is tested. Cross sections are calculated for 1–2000 keV proton impact and good overall agreement is found with available experiments, while some of the results are at variance with a recent model calculation. The single-particle excitation amplitudes are combined in the *LS* coupling scheme to obtain excitation cross sections for particular atomic oxygen configurations. The latter are compared with recent measurements for proton and electron impact. Reasonable agreement is found for many one-electron excitations and some two-electron processes.

PACS number(s): 34.50.Fa, 34.70.+e

I. INTRODUCTION

The recently developed basis generator method (BGM) [1,2] represents a technique to solve the single-electron time-dependent Schrödinger equation for ion-atom collisions in the framework of the independent particle model (IPM) for *N*-electron systems under conditions where probability density is transferred from the target to the continuum as well as to the projectile. It has been tested successfully for such collision systems as $p^{\pm}$-Ne [3,4], He^{2+}-Ne [5], and F^{9+}-Ne [6]. An important aspect of the method is the ability to generate dynamically basis states that can represent accurately the state vector $|\psi(t)\rangle$ during the collision with the appropriate amount of probability amplitude in the continuum as well as in states traveling with the projectile. In particular, the method has been shown to propagate properly all initially occupied orbitals involved in the collisions, i.e., the *K* and *L* shells in collision systems with Ne targets, and *K*, *L*, and *M* shells in *p*-Ar collisions [3].

The BGM is built upon a single-particle representation of the target atom, usually in the framework of density functional theory (DFT) [7]. So far most of the results reported have been obtained with a frozen single-particle potential for the target atom. The validity of the frozen-screening potential (or no-dynamic response) approximation was conjectured on the basis of successful calculations of single-electron capture, ionization, and transfer ionization events for collision energies down into the tens of keV/amu range [3–5]. Pilot calculations with dynamic screening indicate, however, a sensitivity of multiple electron transfer or ionization cross sections to dynamic screening effects [4].

The sensitivity of the calculated cross sections to the particular DFT model has been explored previously [3,5]. It was found that the proper cancellation of the self-interaction contributions as obtained in an exchange-only optimized potential method (OPM) was important for collision calculations, resulting in substantially different cross sections from results obtained with Latter-corrected local density approximation or Hartree-Fock-Slater potentials.

An important aspect of the investigation of BGM calculations was the issue of how to extract the information about electron transfer to the projectile and to the continuum. The most sophisticated analysis is based on exclusive probabilities, calculated in the framework of an IPM with Pauli blocking [8] with subsequent summation over all relevant channels to obtain inclusive cross sections. On the other hand, it is possible to perform an inclusive cross section analysis directly based on single-particle transfer and ionization probabilities: this can be done at the level of the statistical atom [9], or at the level of shell-specific probabilities [10]. For many processes the differences between the various evaluations of inclusive cross sections (e.g., for *m*-electron transfer and simultaneous *n*-electron ionization) are small [5]. An exception occurs when spin effects become important (Pauli blocking prohibits triple capture to an *s* subshell, in which case the statistical treatment of this channel is inappropriate). One of the problems not addressed so far in this context is the issue of relatively large multiple electron transfer and ionization cross sections for proton impact calculated by either method of evaluation. In particular, the IPM predictions about double capture (H^- formation), and even triple and higher-order capture (unphysical channel) as well as about double and higher-order ionization are in conflict with experimental observations. This work attempts to shed some light on this problem.

Another aspect that is addressed in this paper is the calculation of target excitation cross sections in the IPM framework. So far, BGM studies for excitation channels have been restricted to one-electron collision systems, where good agreement with other theoretical work and experimental data has been obtained [11]. The investigation of excitation in many-electron atoms requires the extraction of more exclusive transition probabilities than the charge-state analysis described above. The question arises how different levels of

sophistication in the analysis of these transitions affect the results.

The present paper deals with the somewhat complicated proton-oxygen collision system. The complications arise on several fronts.

(1) The oxygen atom represents a system with a partially populated L_{II} shell, and a spin-triplet ground state configuration $(1s^2 2s^2 2p^4\ {}^3P)$. Since we describe the oxygen atom in terms of an ensemble-averaged single-particle potential, the information about the splitting of the configuration in different terms is lost. Nevertheless, the spin polarization and the angular momentum symmetry can be taken into account in the construction of transition probabilities to specific final states.

(2) The ionization potential of atomic oxygen is very close to 0.5 a.u., which results in a resonant single-electron capture channel. The latter property is difficult to model with a spin-independent single-particle model based on first principles (such as the OPM), and we will therefore consider a model potential for the oxygen $L_{\mathrm{I,II}}$ shells in addition to the DFT approach.

Previous studies of the p-O collision system, which is of astrophysical interest, include experimental observations of single capture, single ionization, and transfer ionization by Thompson and co-workers [12,13], and a recent model calculation which yielded somewhat satisfactory results for ionization and capture, but not for transfer ionization [14]. In the high-energy limit the ionization data can be compared with experimental electron impact results [15]. At very low energies theoretical capture data were obtained in a molecular-orbital approach [16], and by means of the so-called electron nuclear dynamics theory [17]. Very recently, experimental results for $2s$-electron ionization and single excitation with and without simultaneous ionization have been reported for the intermediate energy range [18].

The paper is organized as follows. The theoretical approach to the description of p-O collisions is presented in Sec. II. This discussion is split into three parts. We start with a brief discussion of the representation of the p-O collision system in the IPM and the solution of the single-particle equations in terms of the BGM in Sec. II A. A more general discussion of the IPM approach to ion-atom collisions can be found in Ref. [5]. In Sec. II B, we describe the evaluation of capture and ionization cross sections, which correspond to measurements where the final charge states of the projectile and target atoms are determined. Section II C discusses the calculation of more exclusive transitions involving target excitation. Results for capture and ionization cross sections are presented in Sec. III A, while various excitation channels are discussed in Sec. III B, and processes, which include the production of vacancies in the L_{I} subshell, are studied in Sec. III C. We conclude with a summarizing discussion of our results in Sec. IV. Atomic units ($\hbar = m_e = e = 1$) are used throughout.

II. THEORY

A. IPM representation of the p-O collision system

In the IPM it is assumed that the collision system can be represented in terms of a set of time-dependent single-particle equations for the initially occupied orbitals,

$$i\partial_t \psi_i(\mathbf{r},t) = \hat{h}(t)\psi_i(\mathbf{r},t), \quad i = 1,...,M, \tag{1}$$

with the Hamiltonian

$$\hat{h}(t) = -\frac{1}{2}\Delta - \frac{Q_T}{r} - \frac{Q_P}{|\mathbf{r}-\mathbf{R}(t)|} + v_{ee}(\mathbf{r},t). \tag{2}$$

Here, Q_T and Q_P are the charges of the target and the projectile nuclei, where the latter is assumed to move along a classical straight line trajectory $\mathbf{R}(t)$, and v_{ee} denotes the effective mean-field potential due to the electron-electron interaction. As in our previous work, we approximate v_{ee} by a spherical potential that accounts for the electron-electron interaction in the undisturbed ground state of the target atom, but neglects the response of the electronic system in the presence of the projectile.

According to the Kohn-Sham (KS) scheme of DFT for stationary systems, v_{ee} is given as an explicit or implicit functional of the ground state density n_0 [19]. In the present case of atomic oxygen, n_0 results from an ensemble-averaging procedure over the partially filled L_{II} shell as

$$n_0(r) = \sum_{i=1}^{M} f_i |\varphi_i(\mathbf{r})|^2 \tag{3}$$

with

$$f_i = \begin{cases} 2 & \text{for } i = 1s, 2s, \\ 4/3 & \text{for } i = 2p_{-1}, 2p_0, 2p_1, \\ 0 & \text{otherwise.} \end{cases} \tag{4}$$

The orbitals $\varphi_i(\mathbf{r})$ are the solutions of the stationary KS equations for the target Hamiltonian

$$\hat{h} = -\frac{1}{2}\Delta + v_{\mathrm{KS}}([n_0];r) = -\frac{1}{2}\Delta - \frac{Q_T}{r} + v_{ee}([n_0];r) \tag{5}$$

and provide the initial conditions for the time-dependent collision problem (1): $\psi_i(\mathbf{r}, t = t_i) = \varphi_i(\mathbf{r})$.

Obviously, the spin polarization of atomic oxygen is not taken into account in this scheme, since the K and L_{I} shells are assumed to be populated by two equivalent electrons, respectively, and the ensemble average is taken with respect to four equivalent electrons in the L_{II} shell. As a particular DFT model for the solution of the stationary KS equations, we employ the exchange-only OPM [20], which ensures the proper cancellation of self-interaction contributions, but neglects correlation effects, and thus is comparable to full Hartree-Fock calculations [19]. In particular, the OPM yields the eigenvalue $\epsilon^{\mathrm{OPM}}_{\mathrm{O}(2p)} = -0.614$ a.u. for the $2p$ level of oxygen, which has to be compared with the first ionization potential of 0.500 a.u. [21].

In order to check to what extent this discrepancy influences the results of the collision calculation, we also consider a simple model-potential description of atomic oxygen, which is similar to the one used by Hamre *et al.* [14],

$$v_{KS}([n_0];r)\approx v_{\mathrm{mod}}(r)=-\frac{1}{r}(7.15e^{-\alpha r}-0.15e^{-r}+1). \tag{6}$$

This potential exhibits the correct behavior for $r\to 0$ and $r\to\infty$ and gives the eigenvalue $\epsilon^{\mathrm{mod}}_{\mathrm{O}(2p)}=-0.505$ a.u., if one chooses $\alpha=1.96$, thus allowing for resonant electron capture in p-O collisions. In the vicinity of $r=1$ a.u., where the $2p$ orbital exhibits its maximum, the effective charge Z_{eff} varies between $Z_{\mathrm{eff}}=1$ and $Z_{\mathrm{eff}}=4$. The reduced $2p$-level binding energy is obtained by a faster approach toward $Z_{\mathrm{eff}}=1$ for large r values than in the OPM potential.

The effective single-particle equations (1) are propagated in either case (OPM and v_{mod}) in a basis representation obtained from the BGM, which has been introduced in Refs. [1], [2]. The basic idea of this coupled-channel approach is to expand the solutions $\psi_i(\mathbf{r},t)$ of Eq. (1) in a basis which dynamically adapts to the time-dependent problem and thus allows an appropriate representation of the $\psi_i(\mathbf{r},t)$ including their overlap with the continuum and with bound projectile eigenstates within a finite set of functions. In our previous work, we showed that for single-particle Hamiltonians of the type (2) this can be achieved, if the basis consists of a set of bound eigenfunctions of the undisturbed target $\{\varphi^0_v(\mathbf{r})\}$ and BGM states $\{\chi^\mu_v(\mathbf{r},t)\}$, which are constructed by repeated application of the suitably regularized projectile potential W_P onto the set $\{\varphi^0_v(\mathbf{r})\}$,

$$\chi^\mu_v(\mathbf{r},t)=[W_P(\mathbf{r},t)]^\mu\varphi^0_v(\mathbf{r}). \tag{7}$$

While the functions $\{\varphi^0_v(\mathbf{r})\}$ account for the elastic and target excitation channels, the set $\{\chi^\mu_v(\mathbf{r},t)\}$ describes the overlap of the propagated orbitals with the continuum and with traveling projectile states. In particular, the BGM states of higher order μ are capable of generating the two-center geometry and of representing the relevant quasimolecular states [1], and allow an accurate description of collisions at low impact energies. However, the method is not restricted to the adiabatic region, but has been shown to give reliable results for excitation, capture, and ionization from the quasimolecular regime up to the high-energy, perturbative region [4,11].

We emphasize that this versatility is due to the dynamical adaptation of the basis to the time propagation of the system itself and does not require the accurate representation of all channel functions of interest. In fact, the representation of traveling projectile states becomes poorer with increasing velocity, since the increasingly rapid oscillations of these states cannot be resolved within the basis [1]. This does not prohibit the extraction of reliable electron capture transition amplitudes for fast collisions, as long as the basis size suffices to cover that part of Hilbert space that is addressed by the propagated orbitals.

In the present work we include all target eigenstates $\{\varphi^0_v(\mathbf{r})\}$ of the *KLMN* shells and 100 functions from the set $\{\chi^\mu_v(\mathbf{r},t)\}$ up to order $\mu=8$ in the basis

$$|\psi_i(t)\rangle=\sum_{\mu=0}^{8}\sum_{v=1s}^{4f}c^i_{\mu v}(t)|\chi^\mu_v\rangle \quad\text{with}\quad |\chi^0_v\rangle\equiv|\varphi^0_v\rangle. \tag{8}$$

The reduction of the set $\{\chi^\mu_v(\mathbf{r},t),\mu=1,...,8\}$ to 100 functions is necessary in order to ensure that the overlap matrix remains numerically positive definite.

The integration of the single-particle equations (1) is normally started and terminated at times t_i, t_f corresponding to a distance of 30 a.u. between the projectile and target nuclei. For collisions at low projectile energies the propagation is extended to the final separation of 40 a.u. in order to achieve converged results.

At the final time $t=t_f$ the propagated orbitals $\psi_i(\mathbf{r},t)$ are analyzed with respect to bound channel functions of the isolated target and projectile Hamiltonians, respectively. In the case of the target, the corresponding transition amplitudes can be identified with the expansion coefficients $c^i_{0v}(t_f)$ [cf. Eq. (8)], since the functions $\varphi^0_v(\mathbf{r})$ are explicitly included in the BGM basis. For the projection onto traveling hydrogenic states centered on the projectile we use Eqs. (8) and (7),

$$\begin{aligned}c^{iP}_k(t_f)&=\langle\varphi^P_k(t_f)|\psi_i(t_f)\rangle\\&=\sum_{\mu=0}^{8}\sum_{v=1s}^{4f}c^i_{\mu v}(t_f)\langle\varphi^P_k(t_f)|[W_P(\mathbf{r},t_f)]^\mu|\varphi^0_v\rangle,\end{aligned} \tag{9}$$

and calculate the matrix elements that occur on the right side of Eq. (9) numerically. The amplitudes $c^i_{0v}(t_f)$ and $c^{iP}_k(t_f)$ constitute the starting point for the construction of observables of the many-electron scattering system within the IPM.

B. Analysis of capture and ionization processes

As a first step for the evaluation of capture and ionization cross sections, we define single-particle probabilities for attachment to projectile and target atoms, respectively,

$$P^i_p=\sum_{k=1}^{K}|c^{iP}_k(t_f)|^2, \tag{10}$$

$$P^i_t=\sum_{v=1}^{V}|c^i_{0v}(t_f)|^2. \tag{11}$$

In the present case of p-O collisions we have chosen K to include all states associated with the principal quantum numbers $n=1,2,3$. The $n=3$ shell was found to contribute toward the total capture cross section at most at the 1–2% level over the entire energy range. Assuming that the summations include all relevant channels, a single-particle probability for ionization from a given shell P^i_c is defined by the requirement

$$P^i_c=1-P^i_p-P^i_t. \tag{12}$$

In the present case of an atomic oxygen target, we calculate single-particle probabilities (10), (11), and (12) for the $1s$, $2s$, and $2p$ initial states; the latter are averaged according to

$$P^{2p}_{t,p,c}=\frac{1}{3}\sum_{m=-1}^{1} P^{2p_m}_{t,p,c}. \tag{13}$$

This ensures consistency with the ensemble-averaging procedure that is used for the description of the target ground state [cf. Eq. (3) and note that the L_{II} shell is populated by four electrons].

The following remarks are provided to explain the difficulties associated with the evaluation of multiple electron capture (or ionization) events that arise in the IPM. We concentrate on electron capture by protons even though the problems discussed are of a general nature.

In the detailed analysis based on exclusive channel probabilities one projects on single-particle states that represent the states of the final atom, e.g., the hydrogen atom in the case considered. These are proper final states for the single-capture channel. To evaluate double capture (formation of the negative hydrogen ion) one can take the square of the H($1s$) formation probability. This represents a projection on a poor $H^-(1s^2)$ ground state, but is consistent with the IPM model interpretation of the single-particle results. In principle, one could project onto the eigenstates of an asymptotic Hamiltonian achieved in a time-dependent Hartree-Fock calculation. This effective Hamiltonian would correspond to a fractional charge state, based on the average charge transferred from all single-particle orbitals of the original target atom for a given impact parameter. One would find the results for H(nlm) formation less satisfying than from the projection onto true H(nlm) eigenstates, but the multiple capture events would be based on more reasonable orbital projections. In principle, one could determine in this analysis that multiple electron transfer does not always lead to bound states [e.g., $H^-(1s,nlm)$ could be treated as unbound], but the entire analysis would be very cumbersome.

Another procedure would be to use the amplitudes for H(nlm) production in order to calculate the occupation probability of a correlated H^- state expanded in an atomic hydrogen basis. According to the work of Martín and Salin for target excitation [22], such a procedure would be justified by the fact that electron correlations act on a longer time scale than the collision time.

The less detailed analysis based on trinomial statistics for the capture of m electrons and the simultaneous transfer of n electrons from the target to the continuum can be calculated from the single-particle probabilities for attachment to the projectile (10), to the target (11), and to the continuum (12) (the shell index is suppressed in the following discussion),

$$P_{m,n}=\frac{N!}{m!n!(N-m-n)!}P_p^m P_c^n P_t^{N-m-n}. \tag{14}$$

N denotes the number of electrons in the given shell. The evaluation of charge-state-correlated probabilities based on trinomial shell probabilities is straightforward and in close agreement with the detailed state-dependent (exclusive) analysis, as long as Pauli blocking in the final states is of minor importance [5]. One of the obvious difficulties is the fact that higher-order event probabilities are linked in a direct way to the single-electron event probabilities. While the latter are usually described well by the BGM-IPM calculations, the former are in fact badly overestimated for proton impact. Even though one may simply ignore the multiple capture events as unphysical, it remains as an unsatisfying feature that the conservation of total probability relies on the presence of these higher-order events (as exemplified by net capture and net ionization cross sections in which higher-order events contribute with appropriate multiplicities).

This interpretation problem of distributing N-particle target electron densities over projectile states that cannot accommodate multiple capture events can be exemplified by the proton-oxygen collisions at a low energy (e.g., 5 keV proton impact energy, and the impact parameter of $b=3$ a.u., for which both the single capture and the double capture probabilities peak). The single-particle capture probability corresponds to a total transfer of 0.6 electrons (a single-particle transfer probability of 0.1 in the L shell). Such a relatively low single-particle probability feeds both the single and double capture channels substantially because of the large number of target electrons available. Yet it would be natural to assume that only single-electron capture should be important, and the formation of the negative hydrogen ion should be treated already as an anomaly.

Hamre *et al.* [14] have tried to overcome this difficulty by defining a single-particle capture probability that blocks double (and higher-order) capture. In deriving the expression $P_{1c}=1-(1-P_p)^N$, they have achieved the objective to obtain a single-particle capture probability that has the correct dependence on P_p at small values, and which results in $P_{1c}=1$ in the limit $P_p=1$, so that all multiple capture events are suppressed. The problem with this approach, however, is that the meaning of the expression used by Hamre *et al.* is different from what was intended: it represents the complement of the probability not to capture the electron N times. Why this should be interpreted as the single-capture probability is unclear: in deriving the expression the authors add probabilities for capture that are more inclusive in the other particles to capture probabilities that are gradually less inclusive.

We propose the following alternative to the trinomial analysis, which solves the problem of removing multiple capture in a systematic and meaningful fashion. Suppose we have calculated for the target N-electron system (which could be a single shell) a set of probabilities for capture, ionization, and attachment to the target. We interpret $\hat{P}_p=NP_p$ as the total (fractional) number of electrons captured by the projectile on average at the given impact parameter. Depending on the projectile charge we define as M the number of electrons for a neutral projectile atom (for protons $M=1$). We can now define m-fold capture events by carrying out binomial statistics based on the new single-particle probability $\hat{P}_p/M$,

$$P_m=\frac{M!}{m!(M-m)!}(\hat{P}_p/M)^m(1-\hat{P}_p/M)^{M-m}. \tag{15}$$

This probability when multiplied by the n out of N electron ionization probability,

$$P_n = \frac{N!}{n!(N-n)!} P_c^n (1-P_c)^{N-n}, \tag{16}$$

results in the probability for simultaneous m-fold capture and n-fold ionization. It has the effect of transferring multiple capture probability into the one-electron capture channel if one makes the choice of $M=1$. Other effects include decreased pure single and multiple ionization probabilities, as well as an increased transfer ionization probability.

The analysis in terms of products of binomials [Eqs. (15) and (16)] can be criticized for the following reasons: (a) it works only as long as $NP_p/M<1$—if this probability becomes larger than unity the need arises to somehow define the formation of negative ions; (b) at present it completely neglects capture of more than M electrons; (c) it delineates the capture and ionization processes as competing processes, and has a slight imperfection in the probability conservation (all probabilities would sum to unity if one allowed simultaneous N-electron ionization with M-fold capture, which makes no sense); (d) as a result of (c) it should only be used for $M \ll N$.

It is remarkable how the product of binomial probabilities can remain close to trinomial probabilities: the evaluation procedures of Hamre *et al.* do not give radically deviating results from the present ones when used with the probabilities reported in this paper—according to our calculations the various cross sections for charge-state formation remain comparable with each other within a factor of 2.

The procedure suggested in the present paper to ignore the formation of the negative hydrogen ion by choosing $M=1$ for proton impact is justified *a posteriori* by knowledge of the extremely small measured cross sections in p-Ne collisions [23], while the BGM-IPM calculations with trinomial analysis lead to substantial double capture by proton projectiles. The proposed analysis of a separate projectile space limited to a particle number M resolves the problem of overestimated double capture events only for the choice $M=1$. A choice of $M=2$ (which would allow for the formation of H^-) leads to overestimated double capture as in the trinomial analysis. This follows from treating double capture as the square of the single-electron capture probability. Even the treatment of H^- as a correlated state expressed in an expansion of products of single-particle configurations does not lead to an order-of-magnitude reduction of the H^- formation cross section.

C. Analysis of excitation processes

The statistical approach described in the previous section can also be applied to the calculation of processes that involve target excitation. For example, the probability for exciting n out of N electrons from a specific shell is given by Eq. (16), if the single-particle continuum probability P_c is replaced by a single-particle probability for excitation P_{ex}, which is calculated in analogy to Eq. (11) with the sum restricted to the excited target states of interest. Application of the binomial formula (16) implies that the $N-n$ electrons that are not excited can occupy any other channel, i.e., they can remain bound to the target or they can be transferred to the projectile or the continuum. On the other hand, the final states of these electrons are also controlled in a typical excitation experiment, where either the energy loss of the projectile or the radiation from the excited state is measured, i.e., excitation measurements are normally exclusive.

In the simplest case, an experimentally investigated process can be interpreted within the IPM as the excitation of a single electron with the other electrons being spectators, which do not undergo any transitions but form a $(1s^2 2s^2 2p^3)$ configuration. The evaluation of the corresponding transition probability requires that the terms $(1-P_{\mathrm{ex}})$ in the binomial formula (16) be replaced by single-particle probabilities for elastic scattering P_{el}, resulting in

$$P_1 = NP_{\mathrm{ex}} P_{\mathrm{el}}^{N-1} \tag{17}$$

for a given shell. This procedure, however, is too restricted, as it excludes processes where two (or more) electrons exchange their initial single-particle states, and thus contribute to the elastic many-electron state. This problem arises due to the improper treatment of the indistinguishability of the electrons in a purely statistical analysis.

A better analysis of these processes is obtained from antisymmetrized many-electron wave functions. In Ref. [8] it has been shown that exclusive and inclusive transition probabilities are given as determinants of the single-particle density matrix, if the propagated state and the final states of interest are represented by single Slater determinants. In the case of atomic oxygen, this formalism requires some modification, since the partially filled L_{II} shell results in a set of degenerate ground-state Slater determinants. To be consistent with the ensemble-averaging procedure for the determination of the ground-state *KS* potential and orbitals, the ensemble of all determinants that can be constructed by distributing four electrons over the L_{II} shell has to be considered. However, it may be advantageous for the analysis to account for the fact that atomic oxygen represents a spin-triplet system by restricting the ensemble to states with the total spin magnetic quantum number $M_S=1$. This leads to three degenerate Slater determinants $|\Psi_K(t)\rangle$ with the initial configurations

$$\begin{aligned} |\Psi_1(t_i)\rangle &= |1s^2 2s^2 2p_{-1}^2 2p_0\uparrow 2p_1\uparrow\rangle, \\ |\Psi_2(t_i)\rangle &= |1s^2 2s^2 2p_{-1}\uparrow 2p_0^2 2p_1\uparrow\rangle, \\ |\Psi_3(t_i)\rangle &= |1s^2 2s^2 2p_{-1}\uparrow 2p_0\uparrow 2p_1^2\rangle, \end{aligned} \tag{18}$$

where $\uparrow$ indicates an unpaired spin-up orbital. The transition probability of the ensemble to a fully specified configuration $|\tilde{f}_1 \cdots \tilde{f}_N\rangle$, which is represented by a single Slater determinant formed from spin orbitals

$$|\tilde{f}_j\rangle = |f_j\rangle |\chi_{\sigma_j}\rangle \tag{19}$$

with channel functions $|f_j\rangle$ and the standard spin functions

$$\chi_{1/2}(2) = \begin{pmatrix} 1 \\ 0 \end{pmatrix}, \quad \chi_{-1/2}(s) = \begin{pmatrix} 0 \\ 1 \end{pmatrix}, \tag{20}$$

reads as

$$P_{\tilde{f}_1\cdots\tilde{f}_N}=\frac{1}{3}\sum_{K=1}^{3}|\langle\tilde{f}_1\cdots\tilde{f}_N|\Psi_K(t_f)\rangle|^2$$
$$=\frac{1}{3}\sum_{K=1}^{3}\begin{vmatrix}\gamma_{11}^{1,K}&\cdots&\gamma_{1N}^{1,K}\\ \vdots&\ddots&\vdots\\ \gamma_{N1}^{1,K}&\cdots&\gamma_{NN}^{1,K}\end{vmatrix}. \quad (21)$$

The elements of the one-particle density matrices for the Kth Slater determinant are given as

$$\gamma_{lm}^{1,K}(t_f)=\langle\tilde{f}_1|\gamma^{1,K}(t_f)|\tilde{f}_m\rangle=\sum_{i=1}^{N}\langle\tilde{f}_1|\tilde{\psi}_i^K(t_f)\rangle\langle\tilde{\psi}_i^K(t_f)|\tilde{f}_m\rangle, \quad (22)$$

where the $|\tilde{\psi}_i^K(t_f)\rangle$ denote the propagated spin orbitals that contribute to the Kth configuration [cf. Eq. (18).]

The probability (21) is thus given as the average of the exclusive probabilities for transitions from the individual degenerate configurations. If degeneracies are present in the final states as well, the corresponding probabilities have to be added.

Accordingly, the inclusive probability of finding q electrons in the subconfiguration $|\tilde{f}_1\cdots\tilde{f}_q\rangle$ while nothing is known about the remaining $N-q$ electrons is given as the average of the ordinary inclusive probabilities that have been discussed in Ref. [8],

$$P_{\tilde{f}_1\cdots\tilde{f}_q}=\frac{1}{3}\sum_{K=1}^{3}P^K_{\tilde{f}_1\cdots\tilde{f}_q}, \quad (23)$$

$$P^K_{\tilde{f}_1\cdots\tilde{f}_q}=\begin{vmatrix}\gamma_{11}^{1,K}&\cdots&\gamma_{1q}^{1,K}\\ \vdots&\ddots&\vdots\\ \gamma_{q1}^{1,K}&\cdots&\gamma_{qq}^{1,K}\end{vmatrix}. \quad (24)$$

The inclusive probabilities can be used to calculate particle-hole probabilities of finding the subconfigurations $|\tilde{f}_1\cdots\tilde{f}_q\rangle$ occupied and $|\tilde{f}_{q+1}\cdots\tilde{f}_L\rangle$ vacant:

$$P^{\tilde{f}_{q+1}\cdots\tilde{f}_L}_{\tilde{f}_1\cdots\tilde{f}_q}=\frac{1}{3}\sum_{K=1}^{3}\left(P^K_{\tilde{f}_1\cdots\tilde{f}_q}-\sum_{\tilde{f}_{q+1}}^{L}P^K_{\tilde{f}_1\cdots\tilde{f}_{q+1}}+\sum_{\tilde{f}_{q+1}<\tilde{f}_{q+2}}^{L}P^K_{\tilde{f}_1\cdots\tilde{f}_{q+2}}\mp\cdots(-1)^{L-q}P^K_{\tilde{f}_1\cdots\tilde{f}_L}\right). \quad (25)$$

This formula is used in the present work for the evaluation of $2s$-hole production (cf. Sec. III C).

The procedure to represent the propagated many-electron state as the ensemble of degenerate Slater determinants (18) can still be criticized, because the O$(2p^4\ ^3P)$ ground-state term consists of states with the total spin magnetic quantum numbers $M_S=-1,0$ in addition to the $M_S=1$ states of Eq. (18). Whereas the $M_S=-1$ states are represented in analogy to Eq. (18) by three single Slater determinants, the correct construction of the $M_S=0$ states would require consideration of appropriate linear combinations of Slater determinants in order to ensure that the states are eigenfunctions of total angular momentum L and spin S. This results in considerably more complicated formulas for the transition probabilities of interest.

Nevertheless, an analysis in terms of states with correct spin and angular momentum properties is desirable, as experimentally not only is the initial state prepared in a definite LS symmetry, but the excited final states can also be distinguished by their LS quantum numbers. Instead of forming the appropriate linear combinations of Slater determinants to describe these states, we make use of angular momentum theory and derive an expression for transitions from the $(2p^4\ ^3P)$ oxygen ground state to singly excited states of the type $(2p^3(S_cL_c)nl\ ^3L_f)$ with $L_c=0$ or $l=0$. Such states have been investigated for proton collisions in a recent experiment [18].

In this analysis the ground-state term of atomic oxygen is composed of a mixture of three possible three-electron core states $(^4S,\ ^2P,\ ^2D)$ to which the fourth electron is coupled such that the $2p^4$ state is antisymmetric. When one electron is excited, different excitations are formed (labeled, e.g., by $3s,3s',3s''$ corresponding to the three cores, respectively). They are energetically distinguishable in a spectroscopy experiment, but assumed to be degenerate in our analysis, which is built on a single set of target orbitals. The analysis accounts fully for the angular momentum coupling of the initial L_{II}-shell electrons, but assumes that the inner-shell electrons are not involved actively in forming the final state. The details can be found in the Appendix.

A rather simple result is obtained under the additional assumption that the population of the (S_cL_c) core of the final state can be approximated by a global probability P_{2p^3} for an elastic transition of three electrons [cf. Eq. (A12)],

$$P_{S_cL_cnl}=N[c(S_cL_c)]^2P_{2p^3}P^{2p}_{\mathrm{ex}(nl)}. \quad (26)$$

Here, $c(S_cL_c)$ is a shorthand notation for the coefficients of fractional parentage $(2p^3\,S_cL_c,2p|\}2p^4\ ^3P)$ (CFPs) [24], and $P^{2p}_{\mathrm{ex}(nl)}$ denotes the single-particle probability for excitation of the state (nl) averaged over the $2p$ initial states according to Eq. (13). The CFPs represent the mixing of the three cores in the ground state and determine how the single-particle excitation probability is split between the excited states corresponding to the different cores. With the natural choice for the three-particle elastic probability $P_{2p^3}=P^3_{\mathrm{el}}$ one arrives at the result that the excitation to the state $(2p^3(S_cL_c)nl\ ^3L_f)$ is given by the simple probability (17) multiplied by the square of the CFP for the particular core. We note that

$$\sum_{S_cL_c}[c(S_cL_c)]^2=1. \quad (27)$$

Thus, in this model the squares of the CFPs directly give the relative strength of the contributions of different cores to the excitation channels.

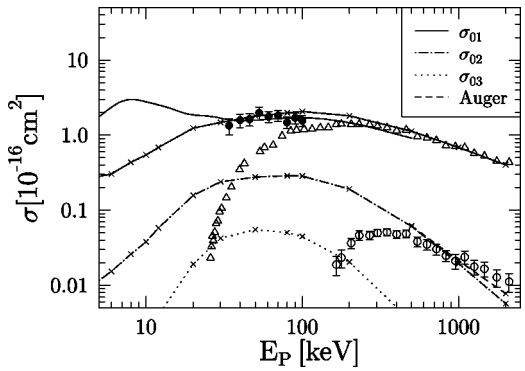

FIG. 1. Total cross sections for single (σ_{01}), double (σ_{02}), and triple (σ_{03}) ionization as a function of impact energy for *p*-O collisions. Theory: full line [14]; lines with crosses, present calculation with OPM potential and trinomial analysis [Eq. (14)]; Auger, (σ_{02}) corrected for Auger processes subsequent to *K*-hole production. Experiment: σ_{01}: (●), [13]; total cross sections for *e*-O collisions σ_{01}: (△) (error bars are smaller than the symbol size); σ_{02}: (○), [15].

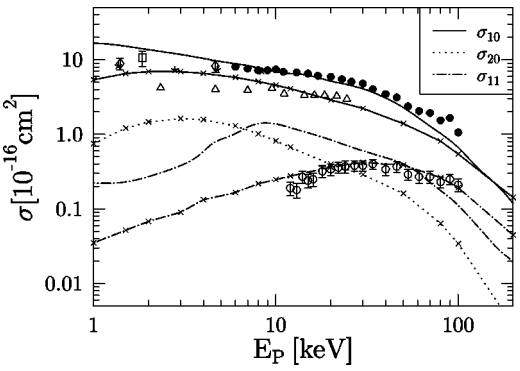

FIG. 2. Total cross sections for pure single (σ_{10}) and double (σ_{20}) capture and transfer ionization (σ_{11}) as a function of impact energy for *p*-O collisions. Theory: lines [14]; lines with crosses, present calculation with OPM potential and trinomial analysis [Eq. (14)]. Experiment: σ_{10}: (●) [12] (error bars are within the symbol size); (△) [26] (error bars are within the symbol size); (⋆) [31]; (□) [32]; (◇) [33]; σ_{11}: (○) [12].

III. RESULTS

As indicated in Sec. II, the time-propagated orbitals obtained with the BGM representation have to be combined appropriately in order to calculate inclusive or exclusive many-electron cross sections. In this section we present results for the following processes Section III A is devoted to the discussion of inclusive ionization, capture, and transfer ionization channels. Exclusive excitation processes involving the promotion of a $2p$ orbital with the final states ($2s^2 2p^3 3s\ ^3S\ ^3P\ ^3D$) as well as the excitation-loss coincidence channel ($2s^2 2p^2 3s\ ^4P\ ^2P$) are analyzed in detail in Sec. III B. Finally, in Sec. III C we investigate processes involving $2s$-vacancy production as the $2s$ to $2p$ excitation channel ($2s2p^5\ ^3P$) or the inclusive electron loss channels ($2s2p^4\ ^2P\ ^4P\ ^2S\ ^2D$). The relevant experimental data are those of Gilbody and co-workers [12,13,26] and Wilhelmi and Schartner [18].

The rather detailed discussion of the results is mainly included to illustrate the theoretical variations that are possible for the final analysis. We compare results obtained on the basis of the OPM and the model potential (6). We compare evaluation in terms of various statistical models and we address the question of Auger and cascade corrections where appropriate.

A. Charge-state-correlated cross sections

We begin with the presentation of results for single and multiple capture and ionization events obtained from BGM calculations with both atomic potentials using the different methods to analyze the single-particle solutions as outlined in Sec. II B. We start the discussion by comparing our results obtained with the OPM potential and shell-specific trinomial statistics with experimental data and the calculations of Hamre *et al.* [14] in Figs. 1 and 2.

Pure ionization has been measured in only a limited energy range in *p*-O collisions. We have therefore included equivelocity *e*-O data [15] in Fig. 1, which provide a meaningful comparison with our cross sections at high energies. In fact, our results for single ionization are in good agreement with the experimental proton data and merge with the electron data at energies $E_P \geqslant 300$ keV. We note that our cross sections do not include contributions from autoionization processes, which occur after specific excitations (cf. Secs. III B and III C). In contrast to the theoretical results of Hamre *et al.* we find no peak structure in the direct ionization at low energies.

Previous work for *p*-Ne collisions [4] indicated that *K* Auger-electron emission should be considered in addition to direct multiple ionization at high impact energies. Within the statistical approach the Auger processes can be taken into account if one assumes that an additional electron is emitted from the target, as soon as one *K* hole is produced in the collision. The corresponding corrected results for total double ionization of oxygen show a slower decrease at high energies than the original data, and are clearly in better agreement with the experimental values for electron impact (cf. Fig. 1). However, it has to be noted that a perfect agreement should not be expected, since electron and proton double ionization cross sections are known to be different even at these high energies [25].

In the low- and intermediate-energy range, the quality of our results for multiple ionization cannot be judged clearly due to the lack of experimental data. However, we conjecture that in analogy to the case of *p*-Ne collisions these cross sections are too large, since the neglected dynamic screening effects should be effective in this region. They are assumed to reduce multiple ionization, because the target potential becomes more attractive as ionization sets in.

The capture and transfer ionization cross sections are displayed in Fig. 2. Our results for the single capture channel lie below most experimental data except for the cross sections reported in Ref. [26]. Since these values are in conflict with the more recent measurements of Ref. [12], they are believed to be incorrect, although no clear explanation for errors in the original measurements was provided [12].

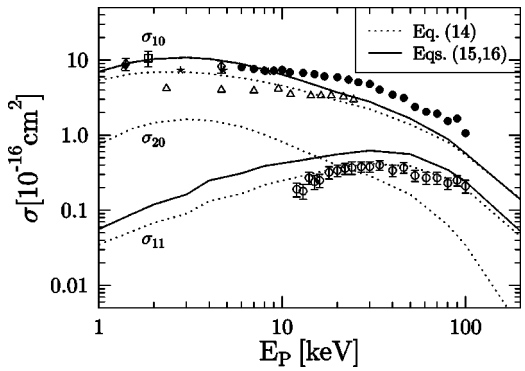

FIG. 3. Total cross sections for pure single (σ_{10}) and double (σ_{20}) capture and transfer ionization (σ_{11}) as a function of impact energy for *p*-O collisions. Theory: present calculation with OPM potential and trinomial analysis [Eq. (14)], and analysis in terms of products of binomials [Eqs. (15) and (16)]. Experiment: same as in Fig. 2.

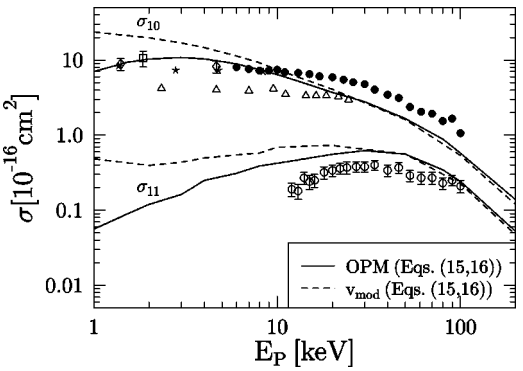

FIG. 4. Total cross sections for pure single capture (σ_{10}) and transfer ionization (σ_{11}) as a function of impact energy for *p*-O collisions. Theory: present calculation with OPM and v_{mod} [Eq. (6)] potentials with analysis in terms of products of binomials [Eqs. (15) and (16)]. Experiment: same as in Fig. 2.

We note that the theoretical results of Hamre *et al.* [14] seem to be in very good agreement with the experimental data of Ref. [12]. However, their evaluation of single capture probabilities has to be criticized, since it is inclusive in the ionization channels (cf. Sec. II). As a consequence, transfer ionization contributions are falsely added to pure capture. We have checked that we also obtain larger capture cross sections if we apply their analysis to our single-particle solutions.

Remarkably, our results for transfer ionization as obtained from trinomial statistics are in good agreement with the experimental data. This is surprising since response effects might be important for this two-electron process, and could reduce the cross sections due to the screening of the projectile and the reduced screening of the target. Only at low energies is there an indication that the calculated cross sections are too large. Why the calculation of Hamre *et al.* [14] results in transfer ionization cross sections at variance with our data and experiment is unclear to us.

In addition, we have included results for double capture in Fig. 2, which have not been measured for atomic oxygen targets. Most certainly, they will overestimate the H^- production cross sections drastically as a consequence of the trinomial analysis.

In the analysis in terms of products of binomials [Eqs. (15) and (16)], this channel and the completely artificial higher-order capture events are removed and the corresponding probabilities are transferred to the single-electron capture channel. The results obtained with this procedure and the OPM potential for v_{KS} are shown in Fig. 3. In the low-energy region ($1\,\mathrm{keV} \leqslant E_P \leqslant 10\,\mathrm{keV}$) we find good agreement with the experimental data if we disregard the measurements of Ref. [26]. A saturation can be observed which might yield too small cross sections at still lower energies, where, however, the validity of the frozen-screening potential approximation is questionable even for single-capture events.

With increasing energy the results due to an analysis in terms of the product of binomials approach the trinomial cross sections. This is due to the fact that higher-order capture probabilities give only small contributions in this region. As a consequence, the single capture falls off too sharply compared to the experimental data of Ref. [12].

As expected, the transfer ionization cross sections obtained with the product of binomials are larger than the trinomial results and lie above the experimental values except at high energies. However, this need not be regarded as a drawback of the analysis, since response effects are expected to reduce the results for this channel with either evaluation procedure. The cross sections for the pure ionization channels remain almost unchanged and therefore are not displayed.

In order to check the sensitivity of the single capture channel to the resonance condition, we have repeated the calculations with the model potential (6), which is chosen to give a substantially better eigenvalue for the $O(2p)$ states (cf. Sec. II A). Corresponding results obtained from the product of binomial analysis are shown in Fig. 4 in comparison with the cross sections for the OPM potential. The single capture as well as transfer ionization cross sections are considerably larger at low impact energies when evaluated with the model potential. No saturation at low energies is observed for the single capture channel. Instead, the cross sections increase with decreasing energy, which is not supported by the experimental data. This behavior shows that the resonant $O(2p)$-$H(1s)$ charge transfer is overemphasized in the model potential approach, since the energy match is fulfilled for all electrons of the oxygen L_{II} shell. Within the trinomial analysis of the single-particle solutions this problem is reflected in a substantial increase of the multiple capture channels.

At higher energies the results approach the OPM values and cross them around 25 keV. It is remarkable that the calculation based on the model potential is unable to boost the single capture cross section at energies above 20 keV. Thus, the discrepancy with the experimental data [12] at higher energies cannot be resolved in the present set of single-particle model calculations. At the same time we note that the transfer ionization cross sections are reproduced reasonably well in our calculations (using the OPM). The results for the pure ionization channels obtained with the

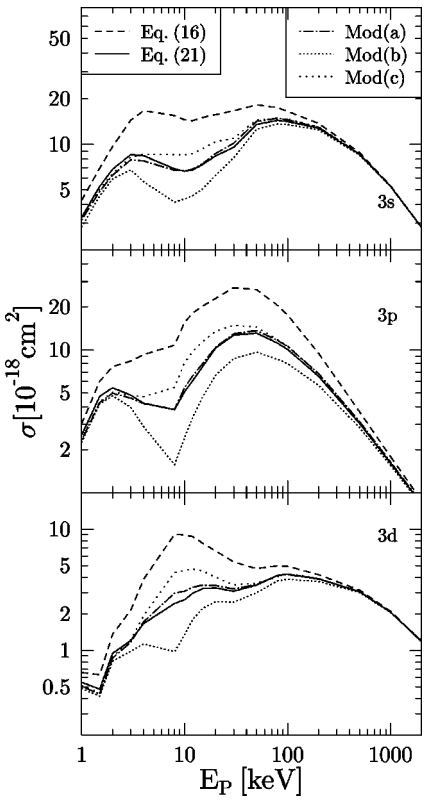

FIG. 5. Total cross sections for single excitation of O($3l$) final states as a function of impact energy for p-O collisions. Theory: present calculation with OPM potential and different analyses according to the cited equations and abbreviations, which are explained in the text.

model potential differ only slightly from the data based on the OPM approach and are not shown.

B. Excitation cross sections

Before we compare our results for specific excitation channels with experimental data, we illustrate the problems and ambiguities that arise when single excitation is analyzed in terms of binomial or related statistical models. To this end, we show in Fig. 5 several sets of results for single excitation to the $3l$ states of oxygen, as obtained with the OPM description of the atomic oxygen ground state while making different assumptions for the behavior of the electrons that are not excited. We emphasize that all data result from the same dynamical calculation and differ only in the methods of extracting the information from the single-particle solutions.

First, we have applied the simple binomial formula (16) for the electrons initially bound to the L_{II} shell. We have then modified this formula according to Eq. (26), which forces three of the four $2p$ electrons to remain in the L_{II} shell throughout the collision [model (a)]. This model is still inclusive with respect to the K-and L_{I}-shell electrons, i.e., the final state of the excited atom is not completely determined. To demonstrate this fact, we have also included the results of a model where Eq. (26) is multiplied by the probabilities for elastic scattering of the inner electrons [model (b)]. This is the most restrictive model for single excitation.

We add to the series of statistical models a variant, where the $N-1$ electrons that are not excited are allowed to populate any single-particle state in the K and L shells [model (c)]. This model accounts for situations where two or more electrons interchange their initial states, but Pauli-forbidden configurations with more than two electrons in the same final state with quantum numbers nlm_l are wrongfully included in the probabilities as well. In addition, the analysis is inclusive with respect to excitation of one or both $2s$ electrons to vacant levels in the L_{II} shell.

Finally, we have performed an analysis in terms of determinants using Eqs. (18) and (21) with summations over all states that correspond to final $(1s^2 2s^2 2p^3 3l)$ configurations. According to the discussion in Sec. II C, this represents the most reliable analysis of single excitation with regard to the indistinguishability of the electrons.

Very similar tendencies can be observed for the three channels $3s$,$3p$,$3d$, which are displayed in Fig. 5. As expected, the binomial formula (16) gives the largest cross sections as it allows $N-1$ electrons to occupy any state except for the excited state of interest. At low and intermediate impact energies, the results of the most restrictive model (b) are smaller by up to a factor of 6. This large difference demonstrates that the solutions of the single-particle equations give rise to various transitions, which are included within the binomial analysis. Partly this could be expected, since capture and ionization are strong reaction channels in this energy range. Only at high impact energies do the two sets of calculations merge to a common curve. This is due to the fact that all inelastic transition probabilities decrease in this region, and the elastic probabilities that are attached to the single excitation probabilities [cf. Eq. (26)] are close to unity. This effect is more pronounced for the dipole-allowed transitions $2p \rightarrow 3s$ and $2p \rightarrow 3d$ than for the dipole-forbidden $2p \rightarrow 3p$ channel, since the dipole-allowed cross sections are mainly due to contributions from large impact parameters, where other inelastic transitions, such as ionization are (almost) negligible.

The results of the analysis in terms of determinants lie between the binomial data and the cross sections of model (b). The remarkable discrepancies with the latter indicate that transitions between states of the L_{I} and L_{II} subshells of oxygen contribute considerably to the final states of type $(1s^2 2s^2 2p^3 3l)$. Obviously, the model (b), where the interchange of particles among these levels is suppressed, is too restrictive to give a suitable description of the corresponding cross sections at moderate impact energies.

The results of the statistical model (a), which requires three $2p$ electrons to remain in the L_{II} subshell but imposes no restriction on the initial $2s$ electrons, are in close agreement with the determinantal cross sections. The crudeness of the model makes this somewhat surprising. Qualitatively, it can be understood as a cancellation of errors, since on the one hand the analysis is too restrictive with respect to the $2p$ electrons, but on the other hand it is too inclusive with respect to the $2s$ electrons (the K-shell electrons are of no importance, as they do not undergo inelastic transitions with noticeable probabilities).

From a theoretical point of view, model (c) is preferable over model (a), since it treats the electrons of both subshells in the same fashion, allowing them to populate any state within the L shell. This method of evaluation gives slightly larger results, mainly as a consequence of adding contributions from processes that include excitations from the $2s$ to the $2p$ subshell. These correspond to many-particle final states with configurations $(1s^2 2s 2p^4 3l)$, which are different from a physical point of view.

We conclude that the diversity of results displayed in Fig. 5 demonstrates that statistical models for the calculation of exclusive transitions have to be employed with some care in the nonperturbative regime. However, the good—though partly accidental and perhaps somewhat fortuitous—agreement of model (a) with the determinantal analysis permits us to exploit this model further for the calculation of excitations with different core states, which can be compared with experimental data. All results presented in the following discussion are obtained from BGM calculations with the OPM potential. We have checked, that the model potential (6) leads to very similar results except at low energies ($E_P \leqslant 10\,\mathrm{keV}$), where, however, no experimental information is available.

In Fig. 6 we show results for the excitations $(2p^3(^4S)3s\ ^3S)$, $(2p^3(^2D)3s'\ ^3D)$ and $(2p^3(^2P)3s''\ ^3P)$, and in Fig. 7 we display the channels $(2p^3(^4S)3p\ ^3P)$ and $(2p^3(^4S)3d\ ^3D)$. According to the preceding discussion and Eq. (26) we describe these transitions by applying model (a) multiplied by the squares of the CFPs that correspond to the particular core states. In addition, we use the more refined analysis of Eqs. (A5), (A7), and (A9), which accounts for the angular momentum coupling in the core. To be consistent with the simple formula (26) we do not attach a probability for elastic scattering of the K- and L_1-shell electrons in this case.

Both analyses give very similar results. The only effect of the more refined model is a slight reduction of the excitations with a ^4S core and a corresponding enhancement of the final states with ^2D and ^2P cores at low impact energies. For intermediate to high energies the splitting of the $3s$ excitation to states corresponding to different cores is completely determined by the CFPs as predicted by Eq. (26). As this result is largely independent of the model potential chosen for the solution of the single-particle equations, we can draw the conclusion that it is a consequence of the IPM description of the collision. In turn, a significant deviation of experimental cross sections from this prediction of the IPM can be interpreted as a signature of (static or dynamic) correlation effects.

Unfortunately, definite conclusions are hampered by the considerable uncertainties in the experimental data. The main problem arises due to the fact that the only measurements for p-O collisions [18] are obtained by fluorescence spectroscopy of the decaying excited states. As a consequence, one has to consider the population of the excited states of interest due to cascades from higher excited states, as well as contributions from competing (autoionizing) decay channels, in order to convert the emission cross sections to the excitation cross sections.

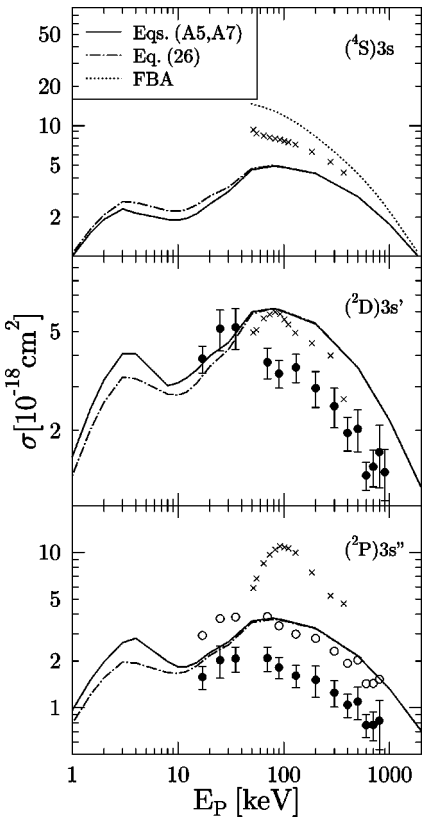

FIG. 6. Total cross sections for excitation of final states $O(2s^2 2p^3(S_c L_c)3s)$ with different cores $(S_c L_c)$ as a function of impact energy for p-O collisions. Theory: present calculation with OPM potential and analyses according to the cited equations; FBA, first Born approximation [30]. Experiment: (●) fluorescence emission cross sections [18]; (○) fluorescence data corrected for autoionization as described in the text; (×) excitation cross sections for e-O collisions [27].

Projectile energy loss measurements for excitation are not blurred by cascades and autoionization processes, but so far have been feasible only for electron impact. We have included corresponding data for e-O collisions [27] in Figs. 6 and 7 for further illustration. We note, however, that they should be compared to the present calculations for proton collisions only on a qualitative level, since the electron and proton data are expected to merge only at the highest energies shown [18]. We add that several experimental investigations based on fluorescence spectroscopy as well as theoretical studies of e-O collisions can be found in the literature, and are discussed along with the new measurements for electron and proton collisions in Ref. [18]. This discussion shows that some of the studies lead to conflicting results, which are not likely to be explained by the uncertainties caused by cascades and autoionization channels in the emission cross sections (cf. the discussion in Ref. [28]).

First, we compare our results with the proton cross sections of Ref. [18] for the $3s$ excitations with different core states (Fig. 6). The experimental emission cross sections for the ^2D and ^2P cores differ in magnitude from the results of our calculations by a factor of 2, but exhibit a similar behavior as a function of projectile energy. However, according to

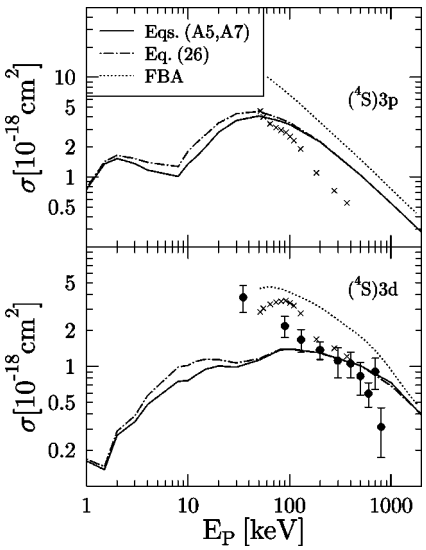

FIG. 7. Total cross sections for excitation of final states $O(2s^2 2p^3(^4S)3p)$ and $O(2s^2 2p^3(^4S)3d)$ as a function of impact energy for *p*-O collisions. Theory: present calculation with OPM potential and analyses according to the cited equations; FBA, first Born approximation [30]. Experiment: (●) fluorescence emission cross sections [18]; (×) excitation cross sections for *e*-O collisions [27].

Ref. [29], the $(2p^3(^2P)3s'')$ state autoionizes with a factor of 0.46, suggesting that the experimental results have to be enhanced by a factor of 1.85 to arrive at the excitation cross section. These modified experimental values agree with our calculations on an absolute scale, but since no enhancement of the $(2p^3(^2D)3s')$ emission cross section due to a competing decay channel can be assumed, the ratio of both cross sections now differs considerably from the prediction of the IPM. In fact, cascades are expected to feed the $(2p^3(^2D)3s')$ population (contributing a fraction of 25%), which would further decrease the experimental results for this channel.

The electron impact measurements of Ref. [27], which are also included in Fig. 6, lie above our calculations for the ^4S and ^2P cores, but with the strong possibility of agreement at high energies. We have performed some additional calculations with a negatively charged projectile (i.e., an antiproton), in order to check if the larger experimental cross sections at intermediate energies can be explained as a charge effect. We do find, however, that the proton and antiproton impact excitation cross sections are very similar for energies $E_P \geqslant 100$ keV.

For the ^2D-core final state the experimental electron impact cross sections are smaller than our values for all impact energies. Together with the larger cross sections for the other cores, it follows that the splitting of the $3s$ excitation to the three cores differs from the IPM prediction. This indicates that correlation effects may be significant, and that in order to understand these excitations one would need at least an atomic oxygen ground state with a different admixture of the $2p^3$ cores than given by the CFPs. However, this cannot be stated with absolute certainty because of the discrepancies between the two experimental data sets and their deviations from other electron impact data.

In addition, we have included the results of a calculation in the first-order Born approximation for electron impact in Fig. 6, which are based on a comparable model potential description of atomic oxygen [30]. Our results merge with the Born values at high energies. This is displayed for the $(2p^3(^4S)3s)$ excitation, but also holds for the other core states, since the splitting of the $3s$ excitation to the three cores is exactly determined by the squares of the corresponding CFPs in the Born approximation (cf. the Appendix).

By contrast, the agreement between our results and the Born cross sections is weak for the $(2p^3(^4S)3p)$ excitation displayed in Fig. 7 (top panel). Although the cross sections of both sets of calculations decrease similarly at high energies, they differ in magnitude by a factor of 1.5. The electron impact measurements of Ref. [27], which are also included, indicate the same asymptotic decrease of the cross section as a function of projectile energy, but the absolute values are considerably smaller than our proton results, which in turn are smaller than the Born cross sections.

For the $(2p^3(^4S)3d)$ excitation, our results merge very well with the Born cross sections at high energies [Fig. 7 (bottom panel)]. This channel was also accessible in the experimental setup of Ref. [18]. Whereas the overall magnitude of the experimental and theoretical cross sections is comparable, we note that the energy dependence is clearly different. Only above an impact energy of 1 MeV do the theoretical results follow the power-law dependence obtained from a fit to the experimental data over the entire energy range. As large cascade contributions to the emission cross section are ruled out by the experimentalists [18], and not much can be learned from a comparison with electron impact data in the intermediate-energy region, the discrepancy cannot be explained at present.

Next, we consider $3s$ excitation with simultaneous loss of one electron from the target atom. Experimental emission cross sections for proton impact are available for the $(2s^2 2p^2(^3P)3s\ ^{2,4}P)$ final states. Due to the removal of one electron from the target, these final states are less exclusive than the ones considered in the discussion above, and would require some modifications in the theoretical treatment. Here, we only apply a simple argument in order to obtain an estimate for the splitting of the $3s$ excitation of the ionized target to the particular core state that was studied experimentally.

According to the IPM, the two-electron process of single excitation and single electron loss proceeds in two independent steps. For example, one electron is removed in the first step and leaves the target ion in one of the three states $(2s^2 2p^3(^4S))$, $(2s^2 2p^3(^2P))$, or $(2s^2 2p^3(^2D))$. Following the arguments given for excitation, we assume that the relative contributions of the three states are given by the corresponding CFPs $(2p^3 S_c L_c, 2p|\}2p^4\ ^3P)$. In the second step, one of the $2p$ electrons is excited to the $3s$ state, which leads to different $2p^2$ cores. We assume again that the splittings are given by the corresponding CFPs $(2p^2 S_c' L_c', 2p|\}2p^3 S_c L_c)$ for each $2p^3$ state. Since we are interested in the total weight for the final states with a $(2p^2(^3P))$ core, we multiply the squares of the CFPs of both

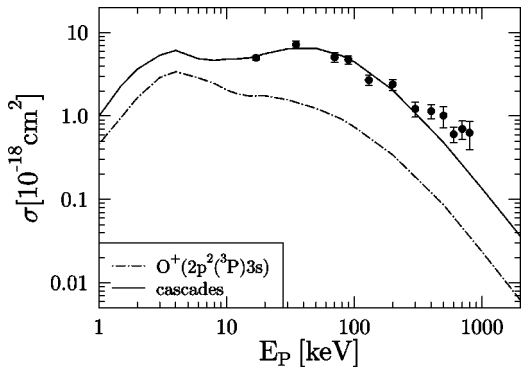

FIG. 8. Total cross sections for transitions to the final state $O^+(2s^22p^2(^3P)3s)$ as a function of impact energy for *p*-O collisions. Theory: present calculation with OPM potential and analyses for direct transitions to $O^+(2s^22p^2(^3P)3s)$, and results including contributions from cascades as described in the text. Experiment: (●) fluorescence emission cross sections [18].

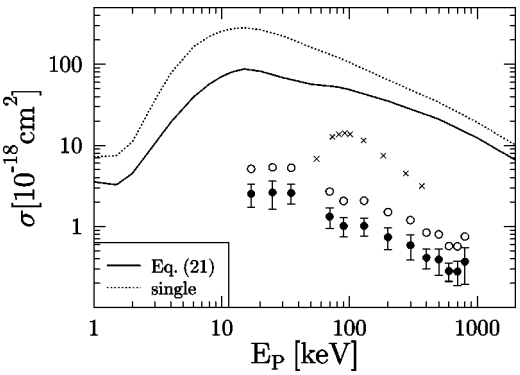

FIG. 9. Total cross sections for excitation of the final state $O(2s2p^5\ ^3P)$ as a function of impact energy for *p*-O collisions. Theory: present calculation with OPM potential and analysis in terms of determinants [Eq. (21)], and single-particle cross section for $2s\rightarrow 2p$ excitation (single); Experiment: (●) fluorescence emission cross sections [18]; (○) fluorescence data corrected for autoionization as described in the text; (×) excitation cross sections for *e*-O collisions [27].

steps for all pathways that lead to this state and sum them up. This gives a factor of 2/3 independent of the order of the two processes, electron loss and excitation. This factor is attached to a modified trinomial probability for simultaneous excitation and electron loss [cf. Eq. (14)],

$$P_{\mathrm{loss}(^3P)3s}=\frac{2}{3}\,\frac{N!}{(N-2)!}(P_p+P_c)P_{\mathrm{ex}(3s)}P_{\mathrm{el}}^2. \qquad (28)$$

As in the calculation of pure single excitation, we assume in Eq. (28) that two $2p$ electrons remain bound to the L_{II} shell of oxygen, whereas the probability is inclusive with respect to the $2s$ electrons.

The results of this model are shown in Fig. 8 along with experimental data, which have been obtained by summation of the three emission cross sections of Ref. [18] that correspond to the $(2s^22p^2(^3P)3s\ ^{2,4}P)$ final states. The experimental values are considerably larger than the calculated cross sections. However, inspection of the Grotrian diagram of singly ionized oxygen reveals that the $(3s\ ^{2,4}P)$ final states can be populated by cascades from various states that correspond to a $3p$ excitation [21]. In fact, some of the corresponding emission lines have been observed in the experiment [18]. In order to take the cascades into account, we have calculated the cross sections for single $3p$ excitation with simultaneous electron loss according to Eq. (28) and added them to the original $3s$ results. In this case, we have omitted the factor 2/3 for the $3p$ excitation, because not only the $(2p^2(^3P)3p)$ state but also states with different cores feed the $(2s^22p^2(^3P)3s\ ^{2,4}P)$ channels.

The results of this analysis are in good agreement with the experimental data (Fig. 8). Only at high impact energies is a slightly different behavior of experimental and theoretical cross sections apparent. We conclude that this two-electron process can be largely understood in terms of an IPM description, if the cascade population of the final state is taken into account. In fact, the experimental emission cross section is dominated by cascades according to our calculations: the cross sections for $3p$ excitation with simultaneous electron loss are larger by a factor of 3 than the corresponding $3s$ values.

C. Transitions with 2*s*-vacancy production

In this section, we present results for processes in which electrons of the L_{I} subshell of atomic oxygen are actively involved. We employ the analysis in terms of the determinants [Eq. (18)] to describe these processes, since it accounts for the coupling of the $2s$ and $2p$ electrons in the final states. This coupling is crucial for the transitions considered. However, the angular momentum properties of neither the propagated nor the final states are taken into account properly in this scheme (cf. Sec. II C). This would require an extension of the analysis described in the Appendix in order to couple the L_{I}-shell electrons to the L_{II}-shell electrons. We have not carried out this extension, since the determinantal analysis should provide a reasonable representation of the processes, as long as one is not interested in the splittings of specific channels into states with different cores.

First, we consider the excitation of a $2s$ electron to a vacant $2p$ state, leading to the final configuration $(2s2p^5\ ^3P)$. Note that final states with different angular momentum quantum numbers do not exist for this process, since the $2p^5$ configuration gives rise to a ^2P term only. The results are shown in Fig. 9 along with experimental data for proton impact [18] and electron impact [27]. We have used Eq. (21) for the analysis of the single-particle solutions obtained from calculations with the OPM potential. In addition to the determinantal results, we show cross sections obtained by a direct integration of the single-particle probabilities for the transition from a $2s$ to a $2p$ state without any combinatorial factor attached. These results include one obvious effect of the Pauli principle, namely, that only one of the $2s$ electrons can be excited to the L_{II} shell, as it is assumed to be populated by three spin-up (↑) and one spin-down (↓) electrons. This effect is included in the determinantal analysis by construction [cf. Eq. (18)].

The single-particle cross sections are larger than the results of the determinantal analysis. Obviously, the former are inclusive in the L_{II}-shell electrons, but the difference be-

tween the two curves also reflects another effect of the Pauli blocking in the final many-particle state: the excitation of the $2s\downarrow$ electron is suppressed, since one of three possible final $2p\downarrow$ states is occupied. In fact, at high energies where other effects are negligible, the two curves differ by a factor of 2/3.

The agreement with the experimental data is very poor for this excitation channel. According to Ref. [29], the $(2s2p^5\ ^3P)$ state autoionizes with an autoionization factor of 0.51. Thus, the emission cross sections of Ref. [18] have to be multiplied by a corresponding factor of 2.04, but these modified cross sections are still considerably smaller than the electron data of Ref. [27]. This suggests that the autoionization factor could be larger than assumed in Ref. [29], but it is clear that this would not resolve the discrepancies with our results unless the autoionization factor were close to unity. This, in turn, would considerably affect the single-ionization channel, since it would shift a large part of our cross section for $(2s2p^5\ ^3P)$ excitation to the direct ionization cross section (cf. Fig. 1).

At present, we can only speculate about the origin of the discrepancies for the $(2s2p^5\ ^3P)$ excitation channel. According to the results of Sec. III B, it is not likely that the theoretical cross sections would be considerably reduced if the analysis were performed in terms of angular momentum eigenstates. Moreover, the following discussion of processes involving electron removal from the target along with the specification of $2s$-hole production supports the strong coupling between the $2s$ and $2p$ states that is the basis for the large cross sections for the $(2s2p^5\ ^3P)$ excitation. One possible source of error in the calculations is the representation of the final state in terms of the orbitals of the ground-state atomic oxygen problem. It may be conjectured that a more accurate description of the final state (including correlation) could lead to significantly smaller cross sections for the excitation of this channel.

In the experiments reported in Ref. [18], final states corresponding to a $(2s2p^4)$ configuration have also been observed. Although the different *LS* terms cannot be described rigorously in terms of the determinantal analysis, particle-hole probabilities [Eq. (25)] for specific configurations can be linked to them in the following way.

First, we consider the production of the final states $(2s2p^4\ ^{2,4}P)$. Obviously, the angular momentum state of the $2p^4$ subconfiguration is unchanged in these collision events. In the determinantal analysis this corresponds to final configurations where three spin-up and one spin-down electrons populate the oxygen $L_{\rm II}$ shell as in the initial ensemble [Eq. (18)]. The transition is calculated via the particle-hole probabilities (25), in which these states together with the *K* shell and one $2s$ spin orbital are filled, whereas the other $2s$ orbital and higher excited states are vacant.

In addition, the population of the final states $(2s2p^4\ ^2S,\ ^2D)$ has been measured. These events require that the $2p^4$ subsystem is changed from a ^3P term to a ^1S or a ^1D term during the collision. Within the determinantal analysis, the final spin-singlet states are represented by configurations with two spin-up and two spin-down electrons in the $L_{\rm II}$ subshell. Since we neglect spin flips, the configurations can be produced only by the excitation of the $2s\downarrow$ electron to a vacant $2p\downarrow$ level with simultaneous removal of a $2p\uparrow$ electron from the target.

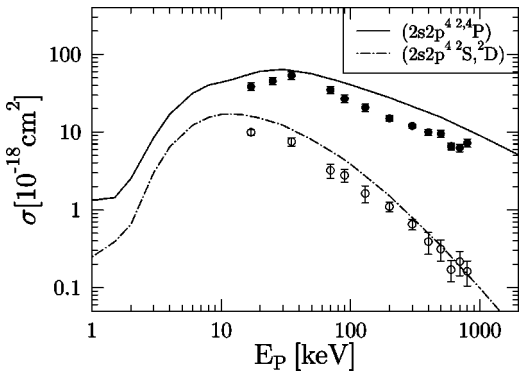

FIG. 10. Total cross sections for transitions to the final states $O^+(2s2p^4\ ^{2,4}P)$ and $O^+(2s2p^4\ ^2S,\ ^2D)$ as a function of impact energy for *p*-O collisions. Theory: present calculation with OPM potential and analysis in terms of particle-hole probabilities [Eq. (25)] as described in the text. Experiment: fluorescence emission cross sections for (●) $O^+(2s2p^4\ ^{2,4}P)$ final states and (○) $O^+(2s2p^4\ ^2S,\ ^2D)$ final states [18].

In Fig. 10 we show our results for the two separate processes in comparison with experimental data, which were obtained by summation of the $(2s2p^4\ ^{2,4}P)$ emission cross sections and the $(2s2p^4\ ^2S,\ ^2D)$ emission cross sections, respectively.

In the latter case, the good agreement of our data with the sum of the experimental cross sections for the ^2S and ^2D final states shows that these events can be largely understood as two-particle processes in the IPM. The remarkable strength of this two-particle process at intermediate energies is caused by the large single-particle probabilities for the $2s\rightarrow 2p$ transition, which directly determine the cross section for the $(2s2p^5)$ excitation discussed above. Thus, the good agreement with the experimental data for the $(2s2p^4\ ^2S,\ ^2D)$ channels is in conflict with the poor agreement for the $(2s2p^5\ ^3P)$ excitation.

In the case of the $(2s2p^4\ ^{2,4}P)$ final states, where the $2p^4$ subsystem is not changed during the collision, our results consist of two contributions corresponding to a vacant $2s\uparrow$ and a vacant $2s\downarrow$ spin orbital, respectively. These contributions differ at intermediate impact energies by up to a factor of 2. This is due to the fact that the $2s\downarrow$ vacancy can be produced by a direct one-particle transition and by a similar two-particle process, as considered for the $(2s2p^4\ ^2S,\ ^2D)$ final states: the excitation of the $2s\downarrow$ electron to the $L_{\rm II}$ shell and the simultaneous removal of the $2p\downarrow$ electron. This process is obviously blocked for the spin-up electrons due to the Pauli principle. At energies $E_P \geqslant 50$ keV, the $2s\uparrow$ and the $2s\downarrow$ vacancy productions merge, which indicates that two-particle processes become unlikely in fast collisions. In this region, the process is mainly due to the direct removal of a $2s$ electron, whereas the $2p$ electrons are merely spectators.

Our results for the sum of $2s\uparrow$ and $2s\downarrow$ vacancy production, which are shown in Fig. 10, lie above the experimental values in the whole energy range. Remarkably, the discrepancies are larger than for the cross sections corresponding to

the $(2s2p^4\ ^2S,\ ^2D)$ final states. This is troublesome insofar as the effects that are neglected in our description (dynamic response, static and dynamic correlation) should be less important for one-electron processes than for two-electron processes.

We note that we have previously observed deviations between theory and experiment for $2s$-vacancy production in p-Ne collisions that are similar to the present results for the $(2s2p^4\ ^{2,4}P)$ final states. These deviations have been attributed to electron correlations that go beyond the simple orbital picture [4]. Given the results presented in this section, it may be conjectured that correlation effects play an important role for processes in which L_{I}-subshell electrons are actively involved. At present, it is not clear how the inclusion of correlation could correct the theoretical results in such a way that the experimental cross sections shown in Figs. 9 and 10 can be explained by a single calculation.

IV. CONCLUSIONS

In this work we have investigated ionization, capture, and excitation in p-O collisions over a broad range of impact energies. We have described the collision system in the IPM framework with a spin-averaged exchange-only OPM potential for the atomic oxygen ground state and have propagated the ensuing set of single-particle equations with the BGM. Emphasis has been given to the question of how to extract physical information about the various inelastic transition channels from the single-particle solutions.

In the case of the rearrangement processes of capture and ionization, we have proposed an analysis in terms of products of binomials as an alternative to the widely used trinomial analysis, which gives rise to significant cross sections for unphysical channels such as multiple capture. In the analysis in terms of products of binomials, the higher-order capture contributions are distributed over the physical capture channels, i.e., they are transferred to the single capture channel in the case of proton impact. The ionization and transfer ionization probabilities are also modified, but in fact they differ only slightly from the trinomial values.

We find very good agreement with experimental data for pure ionization over a broad energy range and somewhat larger cross sections than reported by the experimentalists for transfer ionization from low to intermediate energies. These deviations can be attributed to the neglect of dynamic screening effects in our description. In the case of single capture, the experimental cross sections are well reproduced by our results obtained from the analysis in terms of products of binomials for low impact energies $E_P \leqslant 10$ keV, but our data lie below the recent measurements of Thompson and coworkers for faster collisions. We have shown that this discrepancy is not caused by the energy difference between the initial $2p$ target orbitals and the final projectile ground state that arises as a consequence of the spin-averaging procedure and neglect of correlation effects in the exchange-only OPM. In fact, the model potential (6), which fulfills the energy match for these states nearly exactly and thus allows for resonant charge transfer, leads to almost identical results as the OPM potential in this region.

In the case of target excitation the observables that are accessible experimentally correspond to more exclusive transitions and require a more sophisticated analysis than the application of simple statistical formulas. We have calculated single excitations of the $3l$ channels with different core states in the LS coupling scheme, and have studied processes in which $2s$ vacancies are formed, with a description of the electronic system in terms of an ensemble of Slater determinants. Our results agree with most of the experimental excitation cross sections derived from fluorescence measurements within a factor of 2. A remarkable exception has been found for the excitation of the $\mathrm{O}(2s2p^5\ ^3P)$ state, where theory and experiment differ by an order of magnitude. As this discrepancy is not likely to be attributed to a competing autoionizing decay channel, which is included in the excitation but not in the emission cross section, it appears that correlation effects may be important to describe this transition.

The description of a large number of one- and two-electron processes within experimental uncertainties provides further evidence that an IPM approach with frozen screening potential is applicable to proton-atom collisions at intermediate and higher energies. Future work will concentrate on some outstanding issues, such as the rearrangement problem in He^{2+}-O collisions, where a time-dependent screening potential may be needed for a proper description of the collision dynamics.

ACKNOWLEDGMENTS

We thank Dr. E. Engel for making his OPM atomic structure calculations available to us, and Dr. O. Wilhelmi for communicating the experimental results for p-O excitation prior to publication. This work has been supported by Collaborative Research Grant No. 972997 of the NATO International Scientific Exchange Program and the Natural Sciences and Engineering Research Council of Canada. One of us (T.K.) gratefully acknowledges the financial support of the DAAD.

APPENDIX

We consider the matrix element

$$A_{fi} = \langle \Phi_f | \Psi(t_f) \rangle \tag{A1}$$

between the propagated oxygen ground-state term $(2p^4\ ^3P)$ and a final state of the form $(2p^3(S_cL_c)nl\ ^3L_f)$ with $L_c = 0$ or $l = 0$. In what follows, the oxygen ground state is specified by the quantum numbers $L_i = 1, M_{L_i}, S_i = 1, M_{S_i}$, while the final states are characterized by $L_f, M_{L_f}, S_f = S_i, M_{S_f} = M_{S_i}$. Note that the spin quantum numbers are conserved, since the Hamiltonian is spin independent.

The time-propagated N-particle wave function can be written as a linear combination of vector-coupled product states, which consist of a single particle initially bound to the $n_0 l_0 = 2p$ level and an $(N-1)$-particle system corresponding to the initial $2p^3$ configuration:

$$\Psi(x_1\cdots x_N,t_f)=\sum_{S_1L_1}c(S_1L_1)\sum_{M_{S_1}m_{s_0}}\left\langle S_1M_{S_1},\frac{1}{2}m_{s_0}|S_iM_{S_i}\right\rangle \times\sum_{M_{L_1}m_{l_0}}\langle L_1M_{L_1},l_0m_{l_0}|L_iM_{L_i}\rangle\psi_{n_0l_0m_{l_0}m_{s_0}} \times(x_1,t_f)\tilde{\Psi}_{L_1S_1M_{L_1}M_{S_1}}(x_2\cdots x_N,t_f). \quad \text{(A2)}$$

In this equation, $c(S_1L_1)$ are the coefficients of fractional parentage [24]

$$c(S_1L_1)=(2p^3\,S_1L_1,2p|\}2p^4\,{}^3P)=\begin{cases}-\sqrt{1/3} & \text{for } (S_1L_1)={}^4S\\ -1/2 & \text{for } (S_1L_1)={}^2P\\ \sqrt{5/12} & \text{for } (S_1L_1)={}^2D,\end{cases} \quad \text{(A3)}$$

the quantities $\langle J_1M_{J_1},J_2M_{J_2}|JM_J\rangle$ are Clebsch-Gordan coefficients, and x_j denotes the space and spin coordinates of the jth electron ($j=1,...,N=4$). The construction with the CFPs ensures that $\Psi(x_1\cdots x_N)$ is antisymmetric provided the $(N-1)$-particle function $\tilde{\Psi}(x_2\cdots x_N)$ is antisymmetric [34].

For the final state, the vector-coupled products of antisymmetric $2p^3$ cores and an additional electron in the excited level $nl\neq 2p$ are explicitly antisymmetrized by applying the permutation operator $\hat{P}_{1j}$ for electrons 1 and j,

$$\Phi_f(x_1\cdots x_N)=\frac{1}{\sqrt{N}}\left(1-\sum_{j=2}^{N}\hat{P}_{1j}\right)\times\sum_{M_{S_c}m_s}\left\langle S_cM_{S_c},\frac{1}{2}m_s|S_fM_{S_f}\right\rangle \times\sum_{M_{L_c}m_l}\langle L_cM_{L_c},lm_l|L_fM_{L_f}\rangle \times\varphi_{nlm_lm_s}(x_1)\tilde{\Phi}^{2p_3}_{L_cS_cM_{L_c}M_{S_c}}(x_2\cdots x_N). \quad \text{(A4)}$$

Since each permutation gives the same contribution to the amplitude, we obtain

$$A_{fi}=\sqrt{N}\sum_{S_1L_1}c(S_1L_1)\sum_{M_{L_c}m_l}\sum_{M_{L_1}m_{l_0}}\langle L_cM_{L_c},lm_l|L_fM_{L_f}\rangle \times\langle L_1M_{L_1},l_0m_{l_0}|L_iM_{L_i}\rangle c^{n_0l_0m_{l_0}}_{nlm_l}(t_f) \times\langle\tilde{\Phi}^{2p_3}_{L_cS_cM_{L_c}}|\tilde{\Psi}_{L_1,S_1=S_c,M_{L_1}}(t_f)\rangle \quad \text{(A5)}$$

with the single-particle amplitudes

$$c^{n_0l_0m_{l_0}}_{nlm_l}(t_f)=\langle\varphi_{nlm_l}|\psi_{n_0l_0m_{l_0}}(t_f)\rangle. \quad \text{(A6)}$$

We have removed the explicit dependence on spin quantum numbers in Eq. (A5) by using the orthogonality relation for the corresponding Clebsch-Gordan coefficients, which can be applied due to spin conservation ($S_c=S_1, M_{S_c}=M_{S_1}, m_s=m_{s_0}$).

The three-particle overlap occurring in Eq. (A5) can be decomposed in the same fashion by considering the vector-coupled states of single-particle and two-particle functions, where the latter are again written as vector-coupled products of single-particle orbitals. This leads to the expression

$$\langle\tilde{\Phi}^{2p_3}_{L_cS_cM_{L_c}}|\tilde{\Psi}_{L_1,S_1=S_c,M_{L_1}}(t_f)\rangle=\sum_{L_1'S_1'L_c'S_c',S_1'=S_c'}c(S_1'L_1')c(S_c'L_c')\sum_{M_{L_c'}m_{l'}}\sum_{M_{L_1'}m_{l_0'}}\langle L_c'M_{L_c'},l'm_{l'}|L_cM_{L_c}\rangle \times\langle L_1'M_{L_1'},l_0'm_{l_0'}|L_1M_{L_1}\rangle\sum_{m_{l''}m_{l'''}}\sum_{m_{l_0''}m_{l_0'''}}\langle l''m_{l''},l'''m_{l'''}|L_c'M_{L_c'}\rangle \times\langle l_0''m_{l_0''},l_0'''m_{l_0'''}|L_1'M_{L_1'}\rangle c^{n_0'l_0'm_{l_0'}}_{n'l'm_{l'}}(t_f)c^{n_0''l_0''m_{l_0''}}_{n''l''m_{l''}}(t_f)c^{n_0'''l_0'''m_{l_0'''}}_{n'''l'''m_{l'''}}(t_f), \quad \text{(A7)}$$

where all single-particle quantum numbers refer to $2p$ orbitals and the CFPs

$$c(S_1'L_1')=(2p^2\,S_1'L_1',2p|\}2p^3\,S_1L_1) \quad \text{(A8)}$$

can be found in Ref. [24].

The transition probabilities of interest are obtained by inserting Eq. (A7) in Eq. (A5) and averaging and summing the squares of the amplitude (A5) over M_{L_i} and M_{L_f}, respectively, according to

$$P_{S_cL_cnl}=\frac{1}{2L_i+1}\sum_{M_{L_i}M_{L_f}}|A_{fi}|^2. \quad \text{(A9)}$$

A considerable simplification arises if one assumes that

the electrons which form the $2p^3$ parents of the initial state remain frozen throughout the collision,

$$\langle \tilde{\Phi}^{2p_3}_{L_c S_c M_{L_c}} | \tilde{\Psi}_{L_1, S_1 = S_c, M_{L_1}}(t_f) \rangle = \delta_{L_c L_1} \delta_{M_{L_c} M_{L_1}} . \tag{A10}$$

In this case, the amplitude (A5) reduces to

$$A_{fi} = \sqrt{N} c(S_c L_c) \sum_{M_{L_c} m_l m_{l_0}} \langle L_c M_{L_c}, l m_l | L_f M_{L_f} \rangle \times \langle L_c M_{L_c}, l_0 m_{l_0} | L_i M_{L_i} \rangle c^{n_0 l_0 m_{l_0}}_{n l m_l}(t_f). \tag{A11}$$

Insertion of Eq. (A11) in Eq. (A9) leads to the simple result

$$P_{S_c L_c nl} = \frac{N[c(S_c L_c)]^2}{2L_i + 1} \sum_{m_l m_{l_0}} |c^{n_0 l_0 m_{l_0}}_{n l m_l}|^2 = N[c(S_c L_c)]^2 P^{2p}_{\mathrm{ex}(nl)} \tag{A12}$$

for the situations of interest, i.e., $L_c = 0$ or $l = 0$.

The selection rules (A10) arise naturally, if one works in the Born approximation in the many-particle picture, since the perturbing projectile potential can cause only one-electron transitions [30]. However, application of Eq. (A10) is not consistent within the single-particle framework, where each electron is allowed to change its state during the collision. In order to take this fact into account without losing the simplicity of the expression Eq. (A12), one can multiply this probability by a global probability for an elastic transition of three electrons as discussed in Sec. II C.

[1] H. J. Lüdde, A. Henne, T. Kirchner, and R. M. Dreizler, J. Phys. B **29**, 4423 (1996).
[2] O. J. Kroneisen, H. J. Lüdde, T. Kirchner, and R. M. Dreizler, J. Phys. A **32**, 2141 (1999).
[3] T. Kirchner, L. Gulyás, H. J. Lüdde, A. Henne, E. Engel, and R. M. Dreizler, Phys. Rev. Lett. **79**, 1658 (1997).
[4] T. Kirchner, H. J. Lüdde, and R. M. Dreizler, Phys. Rev. A **61**, 012705 (2000).
[5] T. Kirchner, L. Gulyás, H. J. Lüdde, E. Engel, and R. M. Dreizler, Phys. Rev. A **58**, 2063 (1998).
[6] T. Kirchner, H. J. Lüdde, and R. M. Dreizler, Phys. Scr. **T80**, 416 (1999).
[7] R. M. Dreizler and E. K. U. Gross, *Density Functional Theory* (Springer, Berlin, 1990).
[8] H. J. Lüdde and R. M. Dreizler, J. Phys. B **18**, 107 (1985).
[9] I. Ben-Itzhak, T. J. Gray, J. C. Legg, and J. H. McGuire, Phys. Rev. A **37**, 3685 (1988).
[10] M. Horbatsch, Z. Phys. D: At., Mol. Clusters Suppl. **21**, 63 (1991).
[11] A. Henne, H. J. Lüdde, and R. M. Dreizler, J. Phys. B **30**, L565 (1997); T. Kirchner, H. J. Lüdde, O. J. Kroneisen, and R. M. Dreizler, Nucl. Instrum. Methods Phys. Res. B **154**, 46 (1999).
[12] W. R. Thompson, M. B. Shah, and H. B. Gilbody, J. Phys. B **29**, 725 (1996).
[13] W. R. Thompson, M. B. Shah, J. Geddes, and H. B. Gilbody, J. Phys. B **30**, L207 (1997).
[14] B. Hamre, J. P. Hansen, and L. Kocbach, J. Phys. B **32**, L127 (1999).
[15] W. R. Thompson, M. B. Shah, and H. B. Gilbody, J. Phys. B **28**, 1321 (1995).
[16] M. Kimura, J. P. Gu, G. Hirsch, and R. J. Buenker, Phys. Rev. A **55**, 2778 (1997).
[17] M. Hedström, E. Deumens, and Y. Öhrn, Phys. Rev. A **57**, 2625 (1998).
[18] O. Wilhelmi and K.-H. Schartner (unpublished).
[19] E. Engel and R. M. Dreizler, J. Comput. Chem. **20**, 31 (1999).
[20] E. Engel and S. H. Vosko, Phys. Rev. A **47**, 2800 (1993).
[21] A. A. Radzig and B. M. Smirnov, *Reference Data on Atoms, Molecules, and Ions*, Springer Series in Chemical Physics Vol. 31 (Springer, Berlin, 1985).
[22] F. Martín and A. Salin, Phys. Rev. A **54**, 3990 (1996); **55**, 2004 (1997).
[23] R. D. DuBois and S. T. Manson, Phys. Rev. A **35**, 2007 (1987).
[24] B. W. Shore and D. H. Menzel, *Principles of Atomic Spectra* (Wiley, New York, 1968), Chap. 9.
[25] L. H. Andersen, P. Hvelplund, H. Knudsen, S. P. Møller, A. H. Sørensen, K. Elsener, K.-G. Rensfelt, and E. Uggerhøj, Phys. Rev. A **36**, 3612 (1987).
[26] I. D. Williams, J. Geddes, and H. B. Gilbody, J. Phys. B **17**, 1547 (1984).
[27] E. E. Gulcicek, J. P. Doering, and S. O. Vaughan, J. Geophys. Res. **93**, 5885 (1988); their data from several publications have been summarized in [29].
[28] S. Wang and J. W. McConkey, J. Phys. B **25**, 5461 (1992).
[29] R. R. Laher and F. R. Gilmore, J. Phys. Chem. Ref. Data **19**, 277 (1990).
[30] P. A. Kazaks, P. S. Ganas, and A. E. S. Green, Phys. Rev. A **6**, 2169 (1972).
[31] R. F. Stebbings, A. C. H. Smith, and H. Ehrhardt, J. Geophys. Res. **69**, 2349 (1964).
[32] B. van Zyl and T. M. Stephen, in *Proceedings of the 17th International Conference on the Physics of Electronic and Atomic Collisions, Brisbane 1991*, edited by I. E. McCarthy, W. R. MacGillivray, and M. C. Standage (Griffith University, Brisbane, 1991), p. 437.
[33] B. G. Lindsay, D. R. Sieglaff, D. A. Schafer, C. L. Hakes, K. A. Smith, and R. F. Stebbings, Phys. Rev. A **53**, 212 (1996).
[34] I. Lindgren and J. Morrison, *Atomic Many-Body Theory*, Springer Series on Atoms and Plasmas Vol. 3 (Springer, Berlin, 1986), Chap. 8.